Astron. Astrophys. 330, 782–790 (1998)

ASTRONOMY
AND
ASTROPHYSICS

Satellites on the Lyman β line of atomic hydrogen due to H-H$^+$ collisions

N.F. Allard[1,2], **J. Kielkopf**[3], **and N. Feautrier**[1]

[1] Observatoire de Paris-Meudon, Département Atomes et Molécules en Astrophysique, F-92195 Meudon Principal Cedex, France
[2] CNRS Institut d'Astrophysique, 98 bis Boulevard Arago, F-75014 Paris, France
[3] Department of Physics, University of Louisville, Louisville, Ky 40292 USA

Received 24 July 1997 / Accepted 12 September 1997

Abstract. We present new theoretical calculations of the total profile of the atomic hydrogen Lyman β spectral line perturbed by collisions with protons. The variation of the radiative dipole moment during the collision is taken into account. This leads to an increase in the amplitude of the main spectral line satellites.

Key words: line: profiles – stars: white dwarfs

1. Introduction

Satellites on the Lyman β line of atomic hydrogen due to collisions of the neutral atom with protons have been identified in the spectrum of the DA white dwarf star Wolf 1346, as observed with the Hopkins Ultraviolet Telescope (Koester et al. 1996). These structures, as well as the ones observed at 1600 Å and 1400 Å in the Lyman α wing due respectively to quasi molecular absorption of the H_2 and H_2^+ molecules, have been demonstrated to be a very sensitive temperature indicators in DA white dwarfs. This recent discovery provides motivation for the present work in which we investigate the theory of the Lyman β line profile. The satellites in the red wing of Lyman β are in the 1015 to 1075 Å region for which the Far Ultraviolet Spectroscopic Explorer (FUSE) will have maximum sensitivity, so that new observations at these wavelengths are anticipated. Furthermore, Lyman β profiles are also the subject of an ongoing study of the far ultraviolet spectrum of dense hydrogen plasmas.

Holweger, Koester & Allard (1994) showed that the neutral H-H interaction is also responsible for a 1600 Å feature present in Lambda Boo stars. The 1600 Å satellite should be notable in metal poor stars, while the 1400 Å satellite which is due to H-H$^+$ should be visible in hotter stars. The relative strength of these two satellite features depends very strongly on the degree of ionization in the stellar atmosphere, and thus on the stellar parameters T_{eff} and $\log g$.

Consequently the shape of the Lyman α and β wings is a very sensitive diagnostic tool for these parameters, if the most accurate absorption coefficients are available. The improved theoretical calculations by Allard & Kielkopf (1991), Allard & Koester (1992), Allard et al. (1994) have been successfully used for this purpose to interpret IUE and HST spectra by Koester & Allard (1993), Koester et al. (1994) and Bergeron et al. (1995). They also fit the spectra of laser-produced hydrogen plasmas (Kielkopf & Allard 1995). The theoretical calculations of the line profiles used in their analysis were made with methods developed from the unified theory (Anderson & Talman 1956; Allard & Kielkopf 1982). A detailed description of the theory as applied to the shape of the Lyman α line has been given by Allard et. al (1994). Those calculations were based on the assumption that the radiative dipole moment is constant during an atom-ion collision. As emphasized there, this approximation may be questionable.

The aim of the new calculations presented here is to provide line profiles where the variation of the radiative electric dipole moment during the atom-proton collision is taken into account. The variation of the dipole in the region of the formation of the spectral line satellites is shown to alter the amplitude of the satellites. It also permits the inclusion of collision induced transitions in the spectral line profile. The theoretical approach is based on the theory of pressure broadening due to Baranger (1958) developed in an "adiabatic representation" which does not exclude degeneracy of atomic levels (Royer 1974, 1980 and Allard et al 1997). Accurate theoretical molecular potentials are used here to describe the interaction between radiator and perturber: the H_2^+ potentials are taken from Madsen & Peek (1971), and dipole transition moments have been calculated by Ramaker & Peek (1972).

2. Theory

2.1. General expression for the spectrum

We consider a fixed radiating atom surrounded by moving perturbers. The power radiated at the frequency ω by such a system is

$$P(\omega) = \frac{4\omega^4}{3c^3} I(\omega), \tag{1}$$

Send offprint requests to: N. Allard

where c is the velocity of light and $I(\omega)$ is referred to as the spectrum. The spectrum $I(\omega)$ can be written as the Fourier transform (**FT**) of the autocorrelation function $\Phi(s)$

$$I(\omega) = \frac{1}{2\pi}\int_{-\infty}^{+\infty}\Phi(s)e^{-i\omega s}ds, \tag{2}$$

where

$$\Phi(s) = \mathbf{Tr}\mathbf{D}T^{\dagger}(s)\mathbf{D}T(s)\rho \tag{3}$$
$$= \langle \mathbf{D}^{\dagger}(0)\mathbf{D}(s)\rangle_{Av} \tag{4}$$

is the autocorrelation function of $\mathbf{D}(s) = T^{\dagger}(s)\mathbf{D}T(s)$, the dipole moment of the radiator in the Heisenberg representation (Allard & Kielkopf 1982). $T(s)$ is the time evolution operator

$$T(s) = \exp(\frac{-is\mathbf{H}}{\hbar}); \tag{5}$$

H is the total hamiltonian

$$\mathbf{H} = \mathbf{T}_{nucl} + \mathbf{T}_{elec} + V(\mathbf{x},\mathbf{R}), \tag{6}$$

where $\mathbf{T}_{nucl}$ and $\mathbf{T}_{elec}$ are sums of nuclear and electronic kinetic energies, $V(\mathbf{x},\mathbf{R})$ is the interaction between particles, x denotes collectively the set of electronic coordinates (position and spin) plus spin coordinates of the nuclei, while R denotes the set of position coordinates of the nuclei. The density matrix ρ is given by

$$\rho \equiv \frac{e^{-\beta\mathbf{H}}}{\mathbf{Tr}e^{-\beta\mathbf{H}}} \tag{7}$$

where

$$\langle(\,)\rangle_{Av} \equiv \mathbf{Tr}\rho(\,). \tag{8}$$

2.2. Adiabatic representation

The adiabatic or Born-Oppenheimer representation consists of expanding eigenstates $\Psi(x;R)$ of the total hamiltonian **H** in terms of electronic states $\chi_e(x;R)$ corresponding to frozen nuclear configurations,

$$(\mathbf{T}_{elec} + V(\mathbf{x},\mathbf{R}))\chi_e(x;R) = \mathbf{H}_{elec}(R)\chi_e(x;R) \tag{9}$$
$$= E_e(R)\chi_e(x;R). \tag{10}$$

In the above equation, R appears as a parameter, and the eigenenergies $E_e(R)$ are the potential energy of each molecular state $\chi_e(x;R)$, where

$$\Psi(x,R) = \sum_e \psi_e(R)\,\chi_e(x;R). \tag{11}$$

The label e on the electronic state $\chi_e(x;R)$ indicates the atomic state to which the radiator tends when $R\to\infty$. As atomic states are usually degenerate, there are in general several different energy surfaces which tend to a same asymptotic energy as $R\to\infty$. Let us denote by E_i^{∞} and E_f^{∞} the asymptotic initial and final state energies, and call ε_j the subspace of electronic state $\chi_e(x;R)$ such that $E_e(R)\to E_j^{\infty}$ as $R\to\infty$. In the presence of perturbers, we have R-dependent frequencies

$$\omega_{if}(R) \equiv (E_f(R) - E_i(R))/\hbar \tag{12}$$

which tend to the isolated radiator frequency ω_{if} as the perturbers get sufficiently far from the radiator:

$$\omega_{if}(R)\to\omega_{if} \quad \text{as} \quad R\to\infty \tag{13}$$

with

$$\omega_{\alpha} \equiv \omega_{if} \equiv (E_f^{\infty} - E_i^{\infty})/\hbar \tag{14}$$

Let us introduce projectors $\mathbf{P}_e$ selecting out the e^{th} adiabatic component of any $\Psi(x,R)$ (Royer 1980):

$$\mathbf{P}_e\Psi(x,R) = \psi_e\chi_e(x;R). \tag{15}$$

Letting $\mathbf{P}_j = \sum_{e\in\varepsilon_j}\mathbf{P}_e$ be the projector onto the subspace ε_j of electronic states of asymptotic energy E_j^{∞}, we write

$$\mathbf{D} = \sum_{\alpha}\mathbf{D}_{\alpha}, \tag{16}$$

$$\mathbf{D}_{\alpha} \equiv \sum_{e,e'}{}^{(\alpha)}\,\mathbf{P}_{e'}\mathbf{D}\mathbf{P}_e \tag{17}$$

$$\mathbf{D}_{\alpha}(t) \equiv \sum_{e,e'}{}^{(\alpha)}\,e^{\frac{it\mathbf{H}}{\hbar}}\mathbf{P}_{e'}\mathbf{D}\mathbf{P}_e e^{\frac{-it\mathbf{H}}{\hbar}} \tag{18}$$
$$\equiv \sum_{e,e'}{}^{(\alpha)}\,\mathbf{D}_{e'e}(t) \tag{19}$$

where the sum $\sum_{e,e'}^{(\alpha)}$ is over all pairs (e,e') such that $\omega_{e',e}(R)\to\omega_{\alpha}$ as $R\to\infty$. Thus $\mathbf{D}_{\alpha}$ connects all pairs of adiabatic states whose electronic energy differences become equal to ω_{α} as $R\to\infty$. In the absence of perturbers, $\mathbf{D}_{\alpha}$ would be the component of **D** responsible for the radiative transitions of frequency ω_{α}. We note that the projection operators will introduce directly the weighting factors discussed in Allard et al 1994.

3. The correlation and spectral matrices

Introducing the expansion Eq. 16 of **D** in the expression Eq. 4 of $\Phi(s)$, we obtain

$$\Phi(s) = \sum_{\alpha,\beta}\Phi_{\alpha,\beta}(s) \tag{20}$$

where

$$\Phi_{\alpha,\beta}(s) = \mathbf{Tr}\,\rho\,\mathbf{D}_{\alpha}^{\dagger}\,e^{\frac{is\mathbf{H}}{\hbar}}\,\mathbf{D}_{\beta}\,e^{\frac{-is\mathbf{H}}{\hbar}} \tag{21}$$
$$= \langle\,\mathbf{D}_{\alpha}^{\dagger}(0)\,\mathbf{D}_{\beta}(s)\,\rangle_{Av} \tag{22}$$

The line shape is then

$$I(\omega) = \sum_{\alpha,\beta}I_{\alpha,\beta}(\omega) \tag{23}$$

It is convenient to think of the $\Phi_{\alpha,\beta}$ and $I_{\alpha,\beta}$ as elements of two matrices, which we may call the correlation and spectral matrices respectively. The off diagonal terms $I_{\alpha,\beta}(\omega)$, $\alpha \neq \beta$, represent interference between different spectral lines (Baranger 1958-b), arising from avoided crossings between potential curves with different values E_e^∞. We shall neglect these interference terms. Then

$$I(\omega) = \sum_\alpha I_\alpha(\omega) \tag{24}$$

$$\Phi(s) = \sum_\alpha \Phi_\alpha(s) \tag{25}$$

where

$$\Phi_\alpha(s) = \langle\, \mathbf{D}_\alpha^\dagger(0)\, \mathbf{D}_\alpha(s)\,\rangle_{Av} \tag{26}$$

To simplify writing we will drop the subscript Av.

3.1. Unperturbed spectrum and normalization

Using superscripts (0),(1),...,(N) to mean that 0,1,...,N perturbers are present in a (large) volume $\mathscr{V}$ we can write the zero-perturber correlation function as

$$\Phi_\alpha^{(0)}(s) = \phi_\alpha^{(0)}\, e^{i\omega_\alpha s} \tag{27}$$

where

$$\phi_\alpha^{(0)} = \Phi_\alpha^{(0)}(s=0) \tag{28}$$

$$= \langle\, \mathbf{D}_\alpha^\dagger\, \mathbf{D}_\alpha\,\rangle_{Av}^{(0)} = \sum_{e,e'}{}^{(\alpha)}\, \rho_e\, |\mathbf{D}_{ee'}^{(0)}|^2 \tag{29}$$

is the line strength and where $\sum_{e,e'}{}^{(\alpha)}$ sums over pairs (e,e') such that $\omega_{e',e}(R \to \infty) = \omega_\alpha$, the frequency of the isolated radiator.

The time dependence of $\Phi_\alpha(s)$ is determined by $\mathbf{D}_\alpha(s)$, which is the part of the dipole moment which, in the absence of perturbers, oscillates at the frequency ω_α. It is convenient to express $\Phi_\alpha(s)$ in a kind of "interaction representation" by dividing out its zero-perturber behavior, writing

$$\Phi_\alpha(s) = \phi_\alpha^{(0)}\, e^{i\omega_\alpha s}\, \Psi_\alpha(s) \tag{30}$$

Thus the interaction representation correlation function

$$\Psi_\alpha(s) \equiv \frac{\Phi_\alpha(s)}{\Phi_\alpha^{(0)}(s)} \tag{31}$$

contains all the influence of the perturbers on line α. Note that in the absence of perturbers

$$\Psi_\alpha^{(0)}(s) = 1 \tag{32}$$

4. Uncorrelated perturbers approximation

We now assume that the effects of the different perturbers on the line shape are uncorrelated (see Royer 1980 for a general discussion), that is, we approximate $\Psi_\alpha^{(N)}(s)$ by

$$\Psi_\alpha^{(N)}(s) = [\Psi_\alpha^{(1)}(s)]^N \tag{33}$$

where N is the number of perturbers in the volume $\mathscr{V}$, so that $n = N/\mathscr{V}$ is the number density of perturbers, and $\Psi_\alpha^{(1)}(s)$ corresponds to the presence of a single perturber in the large volume $\mathscr{V}$. Now $\Psi_\alpha^{(1)}(s)$ differs from the zero-perturber value $\Psi_\alpha^{(0)}(s)$ =1 only if the single perturber interacts with the radiator during the time interval $(0,s)$, the probability for which is proportional to $1/\mathscr{V}$. So

$$\Psi_\alpha^{(1)}(s) = 1 + \frac{1}{\mathscr{V}} f_\alpha(s), \tag{34}$$

where

$$f_\alpha(s) = \mathscr{V}(\Psi_\alpha^{(1)}(s) - 1) \tag{35}$$

is well-defined as $\mathscr{V} \to \infty$. We thus get

$$\Psi_\alpha^{(N)}(s) = [\,1 + \frac{1}{N}\,\frac{N}{\mathscr{V}}\, f_\alpha(s)\,]^N \tag{36}$$

In the limit $N \to \infty$, $\mathscr{V} \to \infty$, $N/\mathscr{V} = n$, and

$$\Psi_\alpha^{(N)}(s) = e^{n f_\alpha(s)} \tag{37}$$

Let us now denote

$$\mathbf{d}_\alpha(s) \equiv \mathbf{D}_\alpha^{(1)}(s) e^{-i\omega_\alpha s} \tag{38}$$

$$\mathbf{D}_\alpha^{(0)} = \mathbf{D}_\alpha^{(0)}(s) e^{-i\omega_\alpha s} \tag{39}$$

wherein the free evolution $e^{i\omega_\alpha s}$ is factored out. Then,

$$f_\alpha(s) = \mathscr{V}[\,\frac{\Phi_\alpha^{(1)}(s)}{\Phi_\alpha^{(0)}(s)} - 1\,] \tag{40}$$

$$= \mathscr{V}[\,\frac{\langle \mathbf{d}_\alpha^\dagger(0)\mathbf{d}_\alpha(s)\,\rangle}{\phi_\alpha^{(0)}} - 1\,] \tag{41}$$

$$= \mathscr{V}[\,\frac{\langle \mathbf{d}_\alpha^\dagger(0)\,\mathbf{d}_\alpha(s) - \mathbf{D}_\alpha^{\dagger(0)}\,\mathbf{D}_\alpha^{(0)}\,\rangle}{\phi_\alpha^{(0)}}\,] \tag{42}$$

since

$$\phi_\alpha^{(0)} = \langle \mathbf{D}_\alpha^{(0)^2}\,\rangle \tag{43}$$

Substituting Eq. 37 into Eq. 30 and Eq. 25 we see that for a pair of isolated lines, such as Lyman α and β, we have

$$\Phi(s) = \Phi_\alpha(s) + \Phi_\beta(s) \tag{44}$$

$$= \phi_\alpha^{(0)}\, e^{i\omega_\alpha s}\, e^{n f_\alpha(s)} + \phi_\beta^{(0)}\, e^{i\omega_\beta s}\, e^{n f_\beta(s)} \tag{45}$$

We note that $\Psi_\alpha(0) \neq 1$, and correspondingly

$$f_\alpha(0) = \mathscr{V}[\,\Psi_\alpha^{(1)}(0) - 1\,] \neq 0 \tag{46}$$

that is

$$f_\alpha(0) = \mathscr{I} \cdot \frac{\langle \mathbf{d}_\alpha(0)^2 - \mathbf{D}_\alpha^{(0)^2} \rangle}{\langle \mathbf{D}_\alpha^{(0)^2} \rangle} \neq 0 \tag{47}$$

Thus the perturbed line strength $\phi_\alpha^{(0)} e^{n f_\alpha(0)}$ differs from the 'free' line strength $\phi_\alpha^{(0)}$ by the factor $e^{n f_\alpha(0)}$, which is due to the fact that collisions modify the strength of the dipole moment.The density dependent factor $e^{n f_\alpha(0)}$ expresses the fact that the total intensity radiated increases or decreases according as the dipole moment is increased or decreased, on average by the proximity of perturbers ($e^{n f_\alpha(0)}$ corresponds to the factor $e^{n\langle d^2-1\rangle}$ in Eq. 2.15 of Royer 1978, where the non-degenerate case was treated). We may write

$$f_\alpha(s) = f_\alpha(0) + g_\alpha(s) \tag{48}$$

where

$$g_\alpha(s) = f_\alpha(s) - f_\alpha(0) \tag{49}$$

$$= \mathscr{I} \cdot \frac{\langle \mathbf{d}_\alpha^\dagger(0) [\, \mathbf{d}_\alpha(s) - \mathbf{d}_\alpha(0) \,] \rangle}{\langle \mathbf{D}_\alpha^{(0)^2} \rangle} \tag{50}$$

Here $g_\alpha(0)$ =0, so that we finally obtain the 'normalized lineshape' $J_\alpha(\Delta\omega)$ of the isolated line

$$J_\alpha(\Delta\omega) = \mathbf{FT}[e^{n g_\alpha(s)}] \tag{51}$$

where we introduced the frequency

$$\Delta\omega = \omega - \omega_\alpha \tag{52}$$

measured relative to the unperturbed line.

The fundamental result expressing the autocorrelation function for many perturbers in terms of a single perturber quantity $g(s)$ was first obtained by Anderson (1952) and Baranger (1958a) in the classical and quantum cases respectively. Anderson and Baranger assume a constant dipole which is factored out.

4.1. Adiabatic approximation at the one perturber level

We now neglect the fact that T_{nucl} induces transitions between different electronic states, that is, we approximate

$$\mathbf{H}|\chi_e(\boldsymbol{r})\rangle = (\mathbf{T}_{nucl} + \mathbf{H}_{elec})|\chi_e(\boldsymbol{r})\rangle \tag{53}$$

$$\simeq |\chi_e(\boldsymbol{r})\rangle(\mathbf{T}_{nucl} + E_e(\boldsymbol{r})) \tag{54}$$

As shown numerically by Erikson and Sando (1980), use of the adiabatic approximation at the one perturber level does not seem to introduce serious errors. This is contrary to its use at the N perturber level, which would effectively constrain all binary collisions in a particular history to all lock into the same pair potential curve. In the adiabatic approximation at the one-perturber level a particular potential curve is selected only *within* each individual binary collision – but different *binary* collisions within a history can choose pair potentials at random. This adiabatic approximation seems reasonable insofar as the line wings are concerned but may lead to errors in the shift of the line center (Spielfiedel et al (1979)).

In the classical path approximation, when we assume that the perturber follows a rectilinear trajectory at a single mean velocity $\bar{v}$, we get from Eq. 50 (Allard et al 1997):

$$g_\alpha(s) = \frac{1}{\sum_{e,e'}{}^{(\alpha)} |D_{ee'}|^2} \sum_{e,e'}^{(\alpha)} \cdot \int_0^{+\infty} 2\pi\rho d\rho \int_{-\infty}^{+\infty} dx\, d_{ee'}(r(0)) [\, e^{i\int_0^s dt\, V_{e'e}(r(t))} \cdot d_{e'e}(r(s)) - d_{ee'}(r(0)) \,] \tag{55}$$

where $r(t) = [\, \rho^2 + (x + \bar{v}t)^2 \,]^{1/2}$ with ρ the impact parameter of the perturber trajectory.

$$V_{e'e}(\boldsymbol{r}) = V_{e'}(\boldsymbol{r}) - V_e(\boldsymbol{r}), \tag{56}$$

with

$$V_e(\boldsymbol{r}) = E_e(\boldsymbol{r}) - E_e^\infty \tag{57}$$

If we assume that $d(\boldsymbol{r}) \equiv 1$, we recover the expression due to Anderson and Talman (1956).

5. Lyman β in H-H$^+$ collisions

5.1. Transitions contributing to Lyman β

An H_2^+ correlation diagram was constructed for Lyman β. It is an extension to higher states of the work explained in a previous paper (Allard et al 1994). Table 1 gives us the orbitals of the united atom correlated to the n = 1, 2, and 3 levels of the separated atoms. Only transitions between states of opposite parity and having $|\ m - m'\ | = 0, 1$ are dipole allowed. The molecular transitions which contribute to Lyman β are shown in Table 2. Eq. (26) of Allard et al (1994) gives the weight of each transition.

5.2. Diatomic potentials

The adiabatic interaction of the neutral hydrogen atom and a proton is described by potential energies $V(R)$ for each electronic state of the H_2^+ molecule (R denotes the internuclear distance between the radiator and the perturber). Electric dipole transitions between these states are responsible for the line profile. When the difference $\Delta V(R)$ between the upper and lower potentials for a transition presents an extremum $\Delta V_{\rm ext}$, the unified theory predicts that there will be satellites periodically centered at

$$\Delta\omega = k\Delta V_{\rm ext} \tag{58}$$

$$k = 1, 2, 3, \ldots \tag{59}$$

(Allard 1978; Royer 1978; Kielkopf & Allard 1979). Here $\Delta\omega$ is the frequency difference between the center of the unperturbed spectral line and the satellite feature, measured for convenience in the same units as the potential energy difference.

Table 1. Correlation diagram of H_2^+ for Lyman-beta

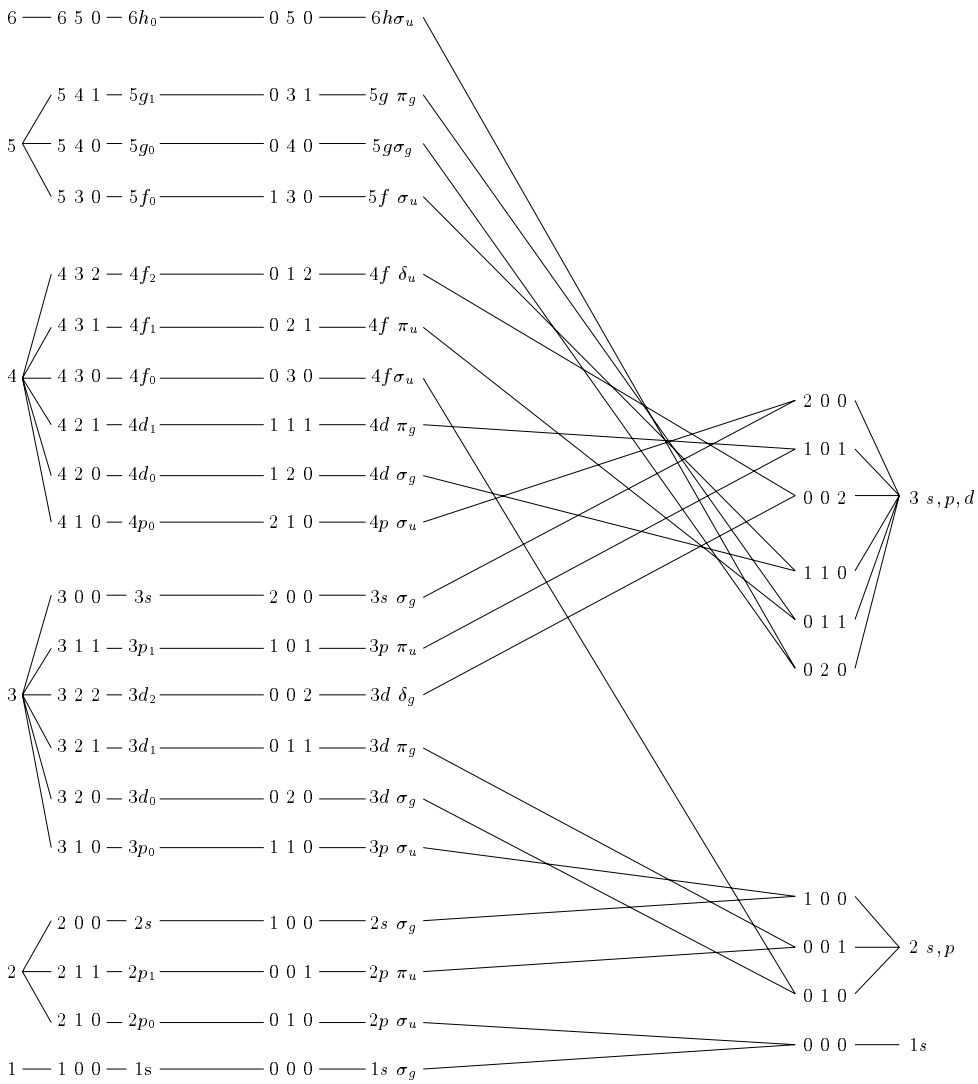

This series of satellites is due to many-body interactions. The k^{th} satellite corresponds to the simultaneous presence of k perturbers in the collision volume. The satellites predicted from the known potential curves of H_2^+ based on difference potential extrema are given in Table 2, where

$$\Delta\omega_{H_2^+} = \Delta V_{\text{ext}} \tag{60}$$

is the frequency of the predicted binary satellite relative to the unperturbed Lyman β line center, and

$$\Delta\omega_{H_3^{++}} = 2\Delta V_{\text{ext}} \tag{61}$$

is the frequency of the three-body satellite. The wavelengths of these satellites are $\lambda_{H_2^+}$ and $\lambda_{H_3^{++}}$. We have used the potentials of H_2^+ calculated by Madsen & Peek (1971) for the transitions contributing to Lyman β, that is, for those that asymptotically go to the n = 3 state of atomic hydrogen and a free proton. Each of the difference potentials for 4 allowed transitions have a minimum which leads us to expect the presence of a corresponding satellite feature in the red wing of Lyman β.

Table 2. Allowed and collisional induced transitions - Satellites due to H-H$^+$ collisions

Upper Level	Lower Level	Weight	$\Delta\omega_{H_2^+}$ (cm^{-1})	$\lambda_{H_2^+}$(Å)	$\Delta\omega_{H_3^{++}}$ (cm^{-1})	$\lambda_{H_3^{++}}$(Å)
$6h\ \sigma_u$	$1s\ \sigma_g$	1	-1185	1037[a]	-2370	1050
			-900	1035[b]	-1960	1046
			-864	1034[c]		
$5g\ \pi_g$	$2p\ \sigma_u$	2	-664	1032[a]		
			-450	1030[b]		
$5g\ \sigma_g$	$2p\ \sigma_u$	1	-5045	1081[a]	-10090	1143
			-4620	1076[b]	-9200	1131
			-4620	1076[c]	-9200	1131
$5f\ \sigma_u$	$1s\ \sigma_g$	1	collisional induced transition			
$4f\ \pi_u$	$1s\ \sigma_g$	2	-3507	1063[a]	-7000	1091
			-3076	1058[b]	-6200	1094
			-3050	1058[c]		
$4d\ \pi_g$	$2p\ \sigma_u$	2				
$4d\ \sigma_g$	$2p\ \sigma_u$	1	collisional induced transition			
$4p\ \sigma_u$	$1s\ \sigma_g$	1				
$3s\ \sigma_g$	$2p\ \sigma_u$	1				
$3p\ \pi_u$	$1s\ \sigma_g$	2				

a) Predicted
b) Individual profile
c) Total profile

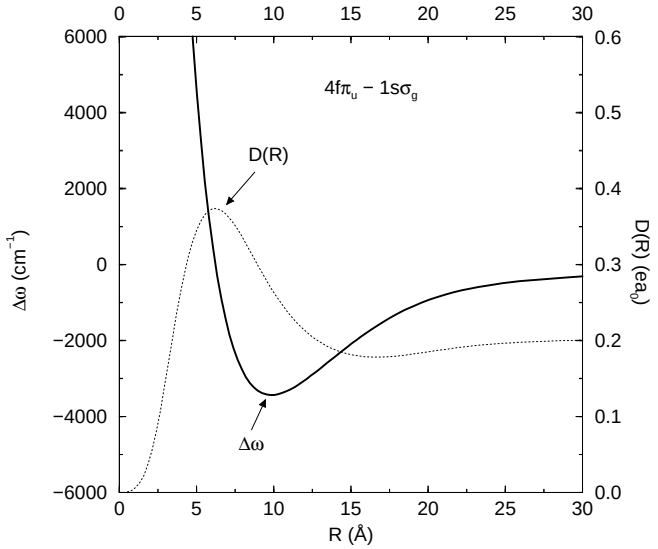

Fig. 1. Difference potential energy $\Delta\omega$ in cm^{-1} and the corresponding $D(R)$ in atomic units for the 1058 Å satellite of Lyman β.

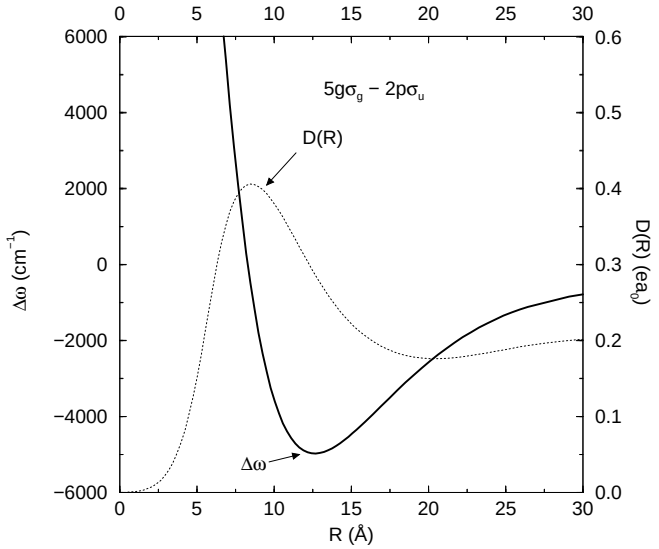

Fig. 2. Difference potential energy $\Delta\omega$ in cm^{-1} in cm^{-1} and the corresponding $D(R)$ in atomic units for the 1076 Å satellite of Lyman β.

5.3. Dipole moments

Dipole transition moments have been calculated as a function of internuclear distance by Ramaker & Peek (1972). To point out the importance of variation of dipole moments on the formation of the satellites, in Figs. 1 to 5 we have displayed $D(R)$ together with the corresponding $\Delta\omega(R)$ for the transitions which should produce satellites on Lyman β.

An examination of Figs. 1 and 2 leads us to expect that there would be an important effect on the amplitude of the 1058 Å

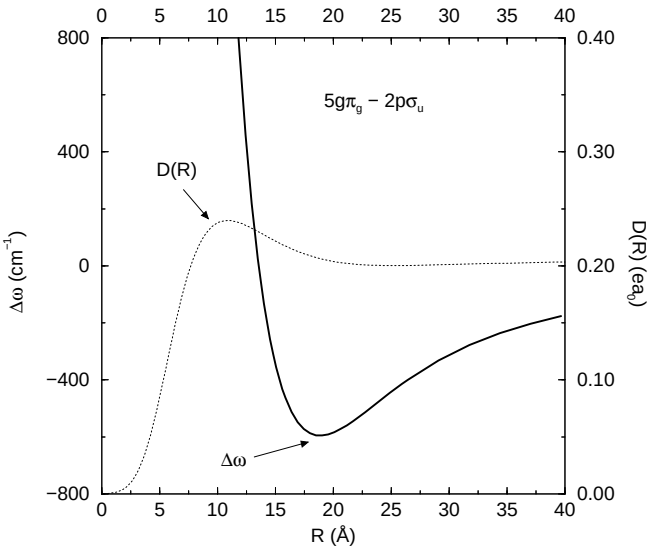

Fig. 3. Difference potential energy $\Delta\omega$ in cm^{-1} and the corresponding $D(R)$ in atomic units for the 1030 Å satellite of Lyman β.

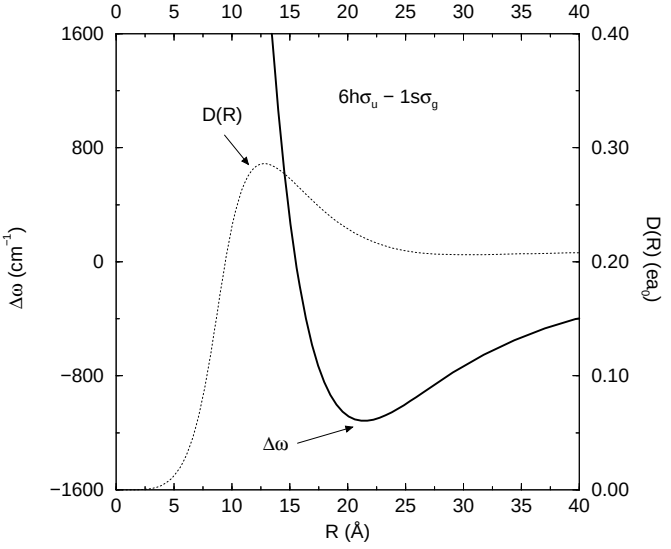

Fig. 4. Difference potential energy $\Delta\omega$ in cm^{-1} and the corresponding $D(R)$ in atomic units for the 1034 Å satellite of Lyman β.

and 1076 Å satellites, as their dipole moments have maximum values which differ notably from the asymptotic values used in the constant dipole approximation. Although the position of this maximum in $D(R)$ is at smaller R than the minimum of the difference potential $\Delta\omega(R)$, the dipole moment increases through the well of the potential responsible of these satellites. By comparison, in Figs 3 and 4 $D(R)$ remains flat with a value close to the asymptotic dipole. Consequently, the variation of the dipole with R should primarily change the satellites at 1058 Å and 1076 Å. Fig. 5, which will be discussed in detail later, shows $D(R)$ for a transition which is asymptotically forbidden.

6. Lyman β profile perturbed by protons

The calculations shown in Fig. 8 have been done at a temperature of 20000 K for different densities of protons from 10^{16} to 10^{18} cm^{-3}. The normalized line shape is the **FT** of the autocorrelation function $J(s)$ given in Eq. (51) where $g(s)$ is calculated in the classical approximation (Eq. (55). We have assumed rectilinear trajectories for the atoms moving with a common relative uniform velocity

$$\bar{v} = (8kT/\pi\mu)^{1/2}, \tag{62}$$

where μ is the reduced mass of the atoms.

In Fig. 6 we have compared the two individual component profiles to the total one for the near wing of Lyman β. The satellite at 1034 Å is a prominent feature. As Fig. 4 shows, the reason for this is that the difference potential energy for this satellite passes through a minimum at a relatively large internuclear distance of 20 Å. As a consequence, the average number of perturbers in the interaction volume is large, leading to a high probability of binary collisions, and making a satellite strong enough to appear distinctly even if quite close to the main line.

In Fig. 7 the profile obtained in the constant dipole approximation is compared to the present calculations. It is interesting to see how much the amplitude for the two calculations differs according to the satellite. As expected, the effect of variable $D(R)$ is only notable for the satellites at 1058 Å and 1076 Å. The dipole variation multiplies the amplitude by a factor 1.16 for the 1058 Å satellite and by 1.58 for the 1076 Å satellite.

The profiles at different densities n_{H^+} are displayed in Fig. 8. These calculations have been done without using the expansion in density which was employed in previous work. Consequently these profiles are valid from the center to the far wing and allow a comparison of the amplitudes of the satellites to the line core.

Multiperturber effects may be apparent in the far wing. To illustrate this, in Fig. 9 we have presented a profile in which the feature at -9200 cm^{-1} is a H_3^{++} satellite due to three-body interactions. The related two-body satellite is at -4620 cm^{-1}. It is the same 1076 Å feature shown in Fig. 8. The other far wing satellite in Fig. 9 at -7700 cm^{-1} is an interference effect. The multiple perturber satellites have different dependences on density from the binary satellites. These features are smeared in the Lyman α blue wing when the Lyman α and Lyman β profiles are summed. (Allard et al 1997).

7. Collision induced absorption

If the electronic states i and f of the isolated radiator are not connected by the dipole moment operator, that is if $D_{if}(R \to \infty) = 0$, allowed radiative transitions cannot occur between these two states. But even in such a case, $D_{if}(R)$ may differ from zero when a perturber passes close to the radiator. In this instance radiative transitions are induced by collisions. Satellites which arise under such circumstances would be absent in the constant D model.

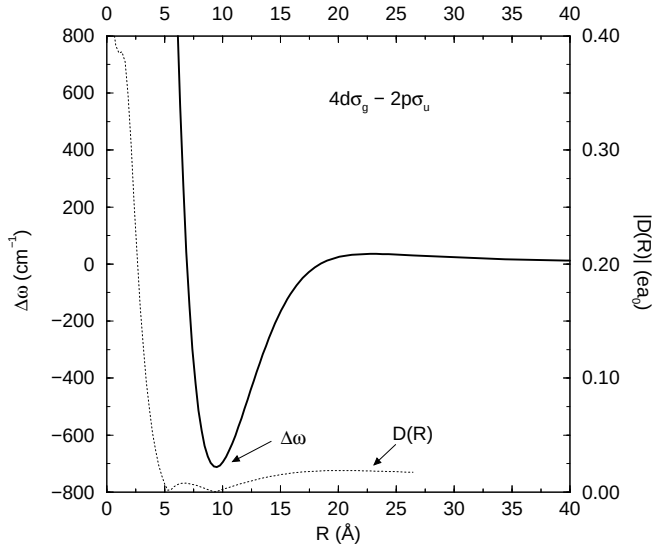

Fig. 5. Variation of the dipole moment with internuclear distance for an asymptotically forbidden transition contributing to the red wing of Lyman β.

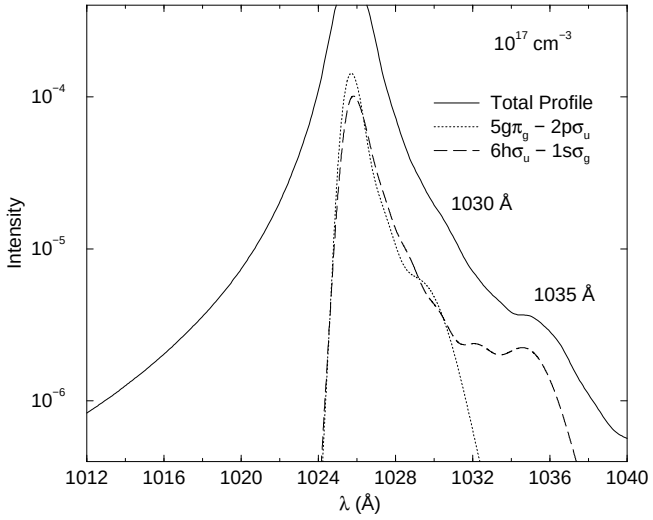

Fig. 6. Near wing of Lyman β.

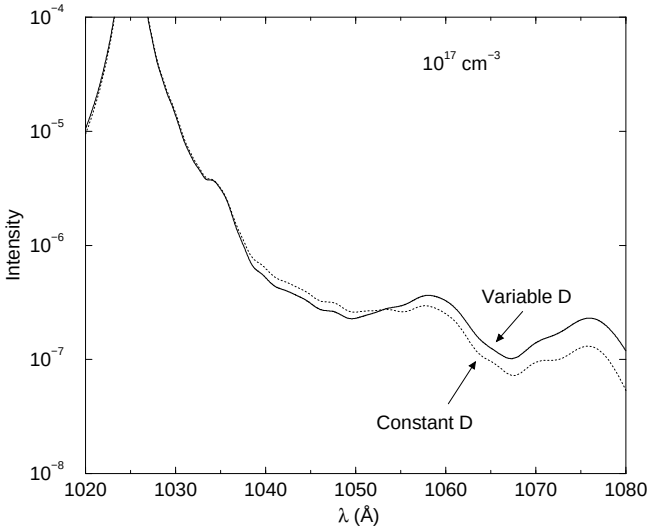

Fig. 7. Comparison of Lyman β profiles with and without variation of dipole moment.

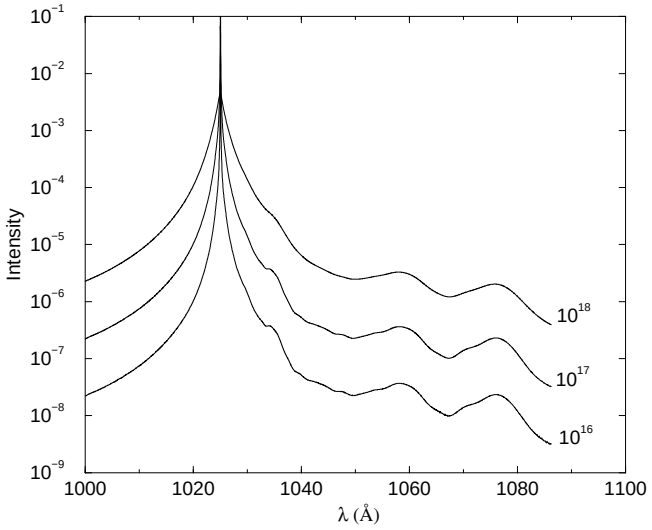

Fig. 8. Comparison of Lyman β profiles with variation of dipole moment at several different densities of H$^+$ in units of cm^{-3}.

For Lyman β there are two asymptotically forbidden transitions $2p\,\sigma_u \rightarrow 4d\,\sigma_g$ and $1s\,\sigma_g \rightarrow 5f\,\sigma_u$ to consider. Fig. 5 shows the potential difference for the $2p\,\sigma_u \rightarrow 4d\,\sigma_g$ transition. The presence of a minimum in $\Delta\omega(R)$ could lead to a satellite feature at 1033 Å but the dipole moment of this transition is quite zero for the internuclear distance R = 10 Å where the potential difference passes through its extremum. Consequently, this forbidden transition gives a small contribution to the profile and in particular it does not produce a satellite, even when the variation of the dipole moment during the collision is included.

8. Conclusion

Satellites structures in the wings of atomic lines can be used as diagnostics of the stellar temperature and gravity. The characteristics of these features (position, amplitude and shape), due to the formation of quasimolecules during collisions between the radiating atom and perturbers, depend directly on the potential energy curves correlated to the atomic levels of the transition (Allard & Kielkopf 1982). Usually, the profiles are calculated assuming that the radiative dipole moment is constant during atom-perturber collisions. As is well known from examples in other radiative processes like spontaneous radiative dissociation (Stephens & Dalgarno 1972), the variation of the dipole moment has to be taken into account to obtain reliable results.

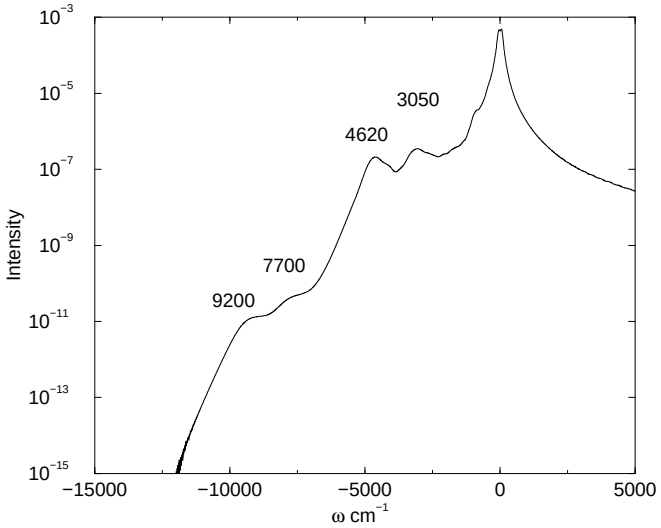

Fig. 9. Multiperturber effects on the far wing, $n_{H^+} = 10^{17}$ cm^{-3}

In the case of Lyman β satellites due to H-H$^+$ collisions, we have shown that large changes (up to 60 %) in the intensity of the satellites may occur when the variation of the dipole moment is taken into account. This effect is important when the dipole moment varies in the region of internuclear distance where the satellite is formed. This result is also valid for other lines. For example, it increases by a factor of 2 the main satellite of Lyman α at 1400 Å due to H-H$^+$ collisions (Allard et al 1997).

Acknowledgements. The work at the University of Louisville is supported by a grant from the U.S. Department of Energy, Division of Chemical Sciences, Office of Basic Energy Sciences, Office of Energy Research.

References

Allard N.F., 1978, J Phys B, 11, 1383
Allard N., Kielkopf J. 1982, Rev Mod Phys, 54, 1103
Allard N.F., Kielkopf J.F., 1991, A&A, 242, 133
Allard N.F., Koester D., 1992, A&A, 258, 464
Allard N., Koester D., Feautrier N., and Spielfiedel A., 1994, A&A 200, 58
Allard N., Royer A., Kielkopf J.F., and Feautrier N., 1997, submitted
Anderson P.W., Talman J.D., 1956, Bell System Technical Publication No. 3117, 29, (Murray Hill, NJ)
Baranger M., 1958a, Phys Rev 111, 481
Baranger M., 1958b, Phys Rev 112, 855
Bergeron P., Wesemael F., Lamontagne R., Fontaine G., Saffer R., Allard N.F., 1995, ApJ, 449, 258
Holweger H., Koester D., Allard N. F., 1994, A&A, 290, L21
Kielkopf J.F., Allard N.F., 1979, Phys Rev Lett 43, 196
Kielkopf J.F., Allard N.F., 1995, ApJ, 450, L75
Koester D., Weidemann E.-M., Zeidler -K.T., Vauclair G.,1985, A&A, 142, L5
Koester D., Allard N.F., 1993, in White Dwarfs: Advances in Observation and Theory, ed. M. Barstow (Kluwer: Dordrecht) p. 237
Koester D., Allard N.F., Vauclair, G., 1994, A&A, 291, L9
Koester D., Finley D. S., Allard N.F., Kruk J.W., Kimble R.A., 1996, ApJ, 463, L93
Madsen M.M., Peek J.M., 1971, Atomic Data, 2, 171
Ramaker D.E., Peek J.M., 1972, J Phys B, 5, 2175
Nelan E.P., Wegner G., 1985, ApJ, 289, L31
Royer A., 1971, Phys Rev A, 3, 2044
Royer A., 1974, Can J Phys, 52, 1816
Royer A., 1978, Acta Phys Pol A, 54, 805
Royer A., 1980, Phys Rev A, 22, 1625
Spielfiedel A, Gilbert D.E., Roueff E., Rostas F., 1979, J. Phys. B, 12, 22
Stephens T.L., Dalgarno A., 1972, JQRST, 12, 589

This article was processed by the author using Springer-Verlag LaTeX A&A style file *L-AA* version 3.